

Dynamic behavior of microscale particles controlled by standing bulk acoustic waves

J. Greenhall, F. Guevara Vasquez, and B. Raeymaekers

Citation: [Applied Physics Letters](#) **105**, 144105 (2014); doi: 10.1063/1.4898012

View online: <http://dx.doi.org/10.1063/1.4898012>

View Table of Contents: <http://scitation.aip.org/content/aip/journal/apl/105/14?ver=pdfcov>

Published by the [AIP Publishing](#)

Articles you may be interested in

[Damping of coherent acoustic vibrations by nanosized pores in colloidal hypersonic crystals](#)

Appl. Phys. Lett. **105**, 051903 (2014); 10.1063/1.4892428

[Controlled rotation of sound-trapped small particles by an acoustic needle](#)

Appl. Phys. Lett. **87**, 094104 (2005); 10.1063/1.2034106

[Erratum: Acoustic radiation force on a compressible cylinder in a standing wave \[J. Acoust. Soc. Am. 116, 201–208 \(2004\)\]](#)

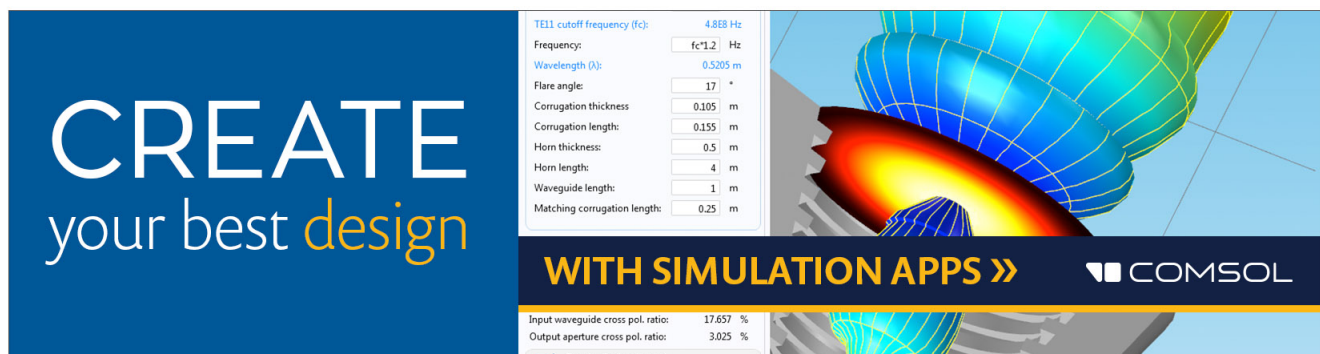
J. Acoust. Soc. Am. **118**, 551 (2005); 10.1121/1.1925848

[Translational motion of a spherical bubble in an acoustic standing wave of high intensity](#)

Phys. Fluids **14**, 1420 (2002); 10.1063/1.1458597

[Acoustic radiation force on a bubble: Viscous and thermal effects](#)

J. Acoust. Soc. Am. **103**, 143 (1998); 10.1121/1.421113

The advertisement features a blue background on the left with the text 'CREATE your best design' in white and yellow. On the right, there is a screenshot of the COMSOL software interface showing a 3D simulation of a horn-like structure with a color gradient from blue to red. A control panel on the left of the screenshot lists various parameters: TE11 cutoff frequency (fc) at 4.868 Hz, Frequency at fc*1.2 Hz, Wavelength (lambda) at 0.5205 m, Flare angle at 17 degrees, Corrugation thickness at 0.105 m, Corrugation length at 0.155 m, Horn thickness at 0.5 m, Horn length at 4 m, Waveguide length at 1 m, and Matching corrugation length at 0.25 m. At the bottom, it says 'WITH SIMULATION APPS >>' and the COMSOL logo. A small status bar at the bottom left shows 'Input waveguide cross pol. ratio: 17.657 %', 'Output aperture cross pol. ratio: 3.025 %', and a checked box for 'Target criterion: passed'.

Dynamic behavior of microscale particles controlled by standing bulk acoustic waves

J. Greenhall,¹ F. Guevara Vasquez,² and B. Raeymaekers^{1,a)}

¹Department of Mechanical Engineering, University of Utah, Salt Lake City, Utah 84112, USA

²Department of Mathematics, University of Utah, Salt Lake City, Utah 84112, USA

(Received 11 September 2014; accepted 1 October 2014; published online 10 October 2014)

We analyze the dynamic behavior of a spherical microparticle submerged in a fluid medium, driven to the node of a standing bulk acoustic wave created by two opposing transducers. We derive the dynamics of the fluid-particle system taking into account the acoustic radiation force and the time-dependent and time-independent drag force acting on the particle. Using this dynamic model, we characterize the transient and steady-state behavior of the fluid-particle system as a function of the particle and fluid properties and the transducer operating parameters. The results show that the settling time and percent overshoot of the particle trajectory are dependent on the ratio of the acoustic radiation force and time-independent damping force. In addition, we show that the particle oscillates around the node of the standing wave with an amplitude that depends on the ratio of the time-dependent drag forces and the particle inertia. © 2014 AIP Publishing LLC.
[\[http://dx.doi.org/10.1063/1.4898012\]](http://dx.doi.org/10.1063/1.4898012)

Non-contact acoustic manipulation of nano- and microscale particles is of critical importance for applications in biology,¹ biomedical devices,² process control,³ and directed self-assembly of nano- and microscale particles.⁴ The acoustic radiation force associated with a standing acoustic wave is used to organize particles dispersed in a fluid medium into user-defined patterns⁴ or manipulate particles to specific locations.⁵ When the radius a of the particles is significantly smaller than the wavelength λ of the acoustic wave (Rayleigh regime) the acoustic radiation force associated with the standing wave drives particles to the nodes ($\Phi > 0$) or antinodes ($\Phi < 0$) of the standing wave, depending on the sign of the acoustic contrast factor for a standing wave,⁶

$$\Phi = \frac{\rho_p - \rho_f}{2\rho_p + \rho_f} - \frac{\rho_f c_f}{3\rho_p (c_{pc}^2 - 4/3c_{ps}^2)}. \quad (1)$$

ρ_f and c_f are the density and sound speed of the fluid medium, and ρ_p , c_{pc} , and c_{ps} are the density and the compression and shear sound speeds of the particle, respectively. In this article, unless otherwise specified, $\Phi > 0$. The acoustic radiation force points toward the nodes of the standing wave, trapping the particles in those locations. Hence, particles can be displaced by changing the location of the nodes through adjustment of the frequency^{7,8} or phase^{5,9,10} of the transducers that create the standing acoustic wave. We consider particle manipulation through adjustment of the transducer phases only, which is typically performed in small increments, while giving the particle sufficient time to reach the new location of the node after each incremental adjustment.⁵ While propagating wave fronts exist within the reservoir, the acoustic radiation force is dominated by the standing waves. As a result, the position of the particle after each phase adjustment is determined as the location where the acoustic pressure amplitude and acoustic radiation force are locally

minimum.^{5,6,9–12} While this method is sufficient for determining the steady-state location of the particles, most industrial and scientific processes require optimizing an objective function, for instance minimizing the time or maximizing the accuracy of the process. Thus, the dynamic characteristics of the fluid-particle system must be identified. The objective of this work is to analyze the trajectory of a spherical particle submerged in fluid, as it is driven to the node of a standing acoustic wave. The transient and steady-state behavior is determined as a function of the particle and fluid properties and the operating parameters of the transducers.

Figure 1 shows a schematic of the set-up. A one-dimensional (1D) reservoir of length L with opposing transducers contains a fluid medium with one particle of radius a , initially located at a node of a standing wave $\varphi(X,t)$. At $t = 0$, a step input to the transducer phases displaces the node over a distance smaller than $\lambda/4$.^{5,9,10} This exposes the particle to a non-zero acoustic radiation force, driving it from its initial position x_0 towards the new node located at x_f , expressed in a local Cartesian coordinate system with origin at the node to which the particle is driven ($X = x_f = 0$). Hence, the displacement of the particle $\Delta x = |x_f - x_0|$ is identical to the

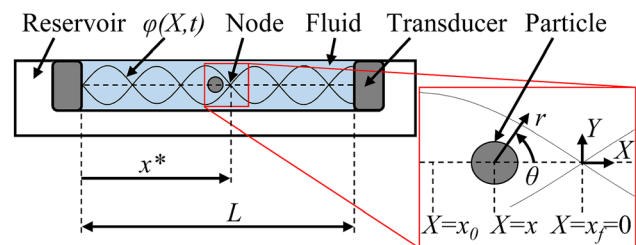


FIG. 1. Cross-sectional view of a fluid reservoir with two opposing transducers, creating a standing acoustic wave $\varphi(X,t)$. The inset image shows a magnified view of the particle located at $X = x$, with respect to the node to which it is driven, located at $X = x_f = 0$. The initial position of the particle $X = x_0$ and the spherical coordinates (r, θ) originating at the center of the particle are defined.

^{a)}bart.raeymaekers@utah.edu

displacement of the node. x^* indicates the position of the node to which the particle is driven, relative to the transducer rather than the local coordinate system. The inset of Fig. 1 shows the particle located at $X = x$, the initial and final positions of the particle, and the spherical coordinate system (r, θ) with origin at the center of the particle.

The dynamics of the fluid-particle system are expressed as

$$m\ddot{x} - F_r(x) - F_d(x, t) = 0, \quad (2)$$

where m is the mass and $\ddot{x} = d^2x/dt^2$ is the acceleration of the particle. F_r is the acoustic radiation force and F_d is the drag force acting on the particle. To calculate F_r and F_d , we first define the acoustic wave in the reservoir. The acoustic wave incident to the particle for the case of a standing plane acoustic wave is written in terms of a velocity potential as

$$\varphi_{in}(X, t) = \Re e(-\varphi_0 e^{i\omega t} i(e^{ikX} - e^{-ikX})), \quad (3)$$

where φ_0 is the amplitude of the standing wave, ω is the operating frequency, and $k = 2\pi/\lambda$ is the wave number. $\Re e(\cdot)$ refers to the real part of Eq. (3). Defining $X = r \cos \theta + x$, with x the location of the particle, Eq. (3) is rewritten in the spherical particle coordinate system as¹¹

$$\varphi_{in}(r, \theta, t) = \Re e\left(\sum_{n=0}^{\infty} A_n j_n(kr) P_n(\cos \theta)\right). \quad (4)$$

Here $j_n(\cdot)$ is the n^{th} order spherical Bessel function of the first kind, $P_n(\cdot)$ is the n^{th} order Legendre polynomial, and

$$A_n = -\varphi_0 e^{i\omega t} (e^{ikx} - (-1)^n e^{-ikx}) (2n+1) i^{n+1}. \quad (5)$$

The scattered wave resulting from the interaction between the acoustic wave and the particle is written as^{6,11,12}

$$\varphi_{sc}(r, \theta, t) = \Re e\left(\sum_{n=0}^{\infty} A_n B_n h_n(kr) P_n(\cos \theta)\right). \quad (6)$$

Here, $h_n(\cdot)$ is the n^{th} order Hankel function of the first kind, and $B_n = \alpha_n + i\beta_n$ is the complex scattering coefficient calculated from the boundary conditions at the fluid-particle interface. The following conditions hold: (i) the fluid pressure is equal to the normal stress at the surface of the particle, (ii) no fluid penetration in the particle occurs, and (iii) the shear stress is zero at the surface of the particle.^{6,11} A complete derivation of the scattering coefficient B_n is given by Faran.¹¹ The resulting acoustic wave in the reservoir is the sum of the incident and scattered wave, $\varphi = \varphi_{in} + \varphi_{sc}$. The acoustic radiation force F_r acting on the particle is calculated from the rate of momentum within a control volume V enclosing the particle,

$$F_r = \oint_V \frac{\partial}{\partial t} (\rho_f \mathbf{u}) dV, \quad (7)$$

where $\mathbf{u} = -\nabla \varphi$ is the 3D velocity vector of the fluid. Chen and Apfel⁶ showed that for the case of a standing wave (Eq. (3)) the acoustic radiation force acting on a spherical particle in the direction of wave propagation (X -direction) is written as

$$F_r = -C_r \sin 2kx, \quad (8)$$

with

$$C_r = 4\rho_f \pi |\varphi_0|^2 \sum_{n=0}^{\infty} (-\beta_n + \beta_{n+1} + 2\alpha_n \beta_{n+1} - 2\beta_n \alpha_{n+1}). \quad (9)$$

Since $ka \ll 1$ (Rayleigh regime), Eq. (9) can be approximated by its low-frequency expansion⁶

$$C_r = 4\rho_f \pi |\varphi_0|^2 (\Phi(ka)^3 + O(ka)^5), \quad (10)$$

where $O(ka)^5$ represents the fifth and higher order terms. In addition, Westervelt¹³ showed that a particle in a standing acoustic wave is subject to Stokes and Oseen forces, i.e., the drag force on the particle caused by velocity difference between the particle surface and the surrounding fluid, given as

$$F_d = C_s(\bar{u} - \dot{x}) + C_o(\bar{u} - \dot{x})|\bar{u} - \dot{x}|. \quad (11)$$

Here $\dot{x} = dx/dt$ is the particle velocity, $C_s = 6\pi\mu a$ and $C_o = 9/4\pi\rho_f a^2$ are the Stokes and Oseen coefficients, respectively, and μ is the dynamic viscosity of the fluid. \bar{u} is the fluid velocity at the particle surface in the X -direction, averaged over $\theta \in [0, \pi]$, i.e.,

$$\bar{u} = -\frac{1}{\pi} \int_0^\pi \left(\frac{\partial \varphi}{\partial r} \cos \theta - \frac{1}{a} \frac{\partial \varphi}{\partial \theta} \sin \theta \right) d\theta. \quad (12)$$

Thus, using $\varphi = \varphi_{in} + \varphi_{sc}$ and Eqs. (4) and (6) we find that

$$\bar{u}(t) = \Re e(u_0 e^{i\omega t} \cos kx), \quad (13)$$

where x is the position of the particle and u_0 is the fluid velocity amplitude, i.e.,

$$u_0 = \Re e\left(-\frac{\varphi_0}{\pi} \sum_{n=0}^{\infty} A_n G_n \left\{ k(j_n'(ka) + B_n h_n'(ka)) + \frac{1}{a} (j_n(ka) + B_n h_n(ka)) \right\}\right). \quad (14)$$

The prime denotes the first derivative of $j_n(\cdot)$ and $h_n(\cdot)$ with respect to ka . G_n is defined as

$$G_n = \begin{cases} 0, & \text{even } n \\ \frac{\Gamma(n/2)\Gamma(n/2+1)}{((n-1)/2)!((n+1)/2)!}, & \text{odd } n, \end{cases} \quad (15)$$

where $\Gamma(\cdot)$ is the Gamma function. Combining Eqs. (2) and (8)–(15) yields the dynamics of the fluid-particle system,

$$m\ddot{x} + C_r \sin 2kx - C_s(\bar{u} - \dot{x}) - C_o(\bar{u} - \dot{x})|\bar{u} - \dot{x}| = 0. \quad (16)$$

Assuming small fluid velocity amplitude u_0 and particle displacement Δx , we linearize Eq. (16), i.e.,

$$\ddot{x} + 2\zeta\omega_n \dot{x} + \omega_n^2 x - C_s \bar{u} = 0, \quad (17)$$

with the damping coefficient $\zeta = C_s/\sqrt{8kmC_r}$, and the natural frequency $\omega_n = \sqrt{2kC_r/m}$. Increasing the amplitude of the standing wave φ_0 increases the fluid velocity amplitude u_0 ,

causing the solution of the linearized system to diverge from that of Eq. (16), resulting in a nonlinear response. The particle will approach the node and then oscillate. The response of the linear system (Eq. (17)) can be solved given the initial conditions $(x(t = 0) = x_0, \dot{x}(t = 0) = 0)$ and is a function of Δx . However, no closed-form solution has been documented in the literature describing the response of the nonlinear system (Eq. (16)). Hence, we numerically simulate the trajectory of a particle while it is driven to the node of the standing wave using a second order Runge-Kutta scheme.

Equation (16) shows that the particle trajectory is defined by a time-independent acoustic radiation force that drives the particle towards the node, and a time-independent Stokes drag force and time-dependent Stokes and Oseen drag forces that resist the particle motion. Once the particle reaches the node of the standing wave, the amplitude of the radiation force and the average velocity of the particle is zero, causing the time-independent Stokes drag force to be zero. Thus, the time-dependent Stokes and Oseen drag force and the particle inertia dominate the dynamics of the fluid-particle system and the particle enters into a stable periodic oscillation with amplitude \tilde{x} around the node. Because the time-dependent terms in Eq. (16) are oscillatory and quasi-reversible over one period T of the standing wave, their effect on the average position of the particle over T is negligible, and the average particle position is dictated by the time-independent radiation force F_r and time-independent Stokes drag force $C_s \dot{x}$. We define the nondimensional variable K_1 as the ratio of the maximum acoustic radiation force that the particle can experience, i.e., when it is located halfway between the node and antinode, and the maximum possible time-independent Stokes drag force, i.e., the drag force when the particle travels at c_f . Hence,

$$K_1 = \frac{\rho_f \varphi_0^2 \Phi(ka)^3}{\mu a c_f}. \tag{18}$$

Adjusting K_1 simultaneously changes ω_n and ζ as $K_1 \sim \omega_n^2$ and $K_1 \sim 1/\zeta^2$. In most applications, it is necessary for a particle to be stationary at a desired location and to minimize oscillation amplitude \tilde{x} around the desired location. To characterize \tilde{x} we define the dimensionless variable K_2 as the ratio of the time-dependent Stokes and Oseen drag forces and the particle inertia for the maximum steady-state particle velocity $\dot{x} = -\bar{u}$. Hence,

$$K_2 = \frac{\mu + \varphi_0 \rho_f k a}{\omega \rho_p a^2}. \tag{19}$$

The transient and steady-state response of the system is controlled by altering the forces acting on the particle, through adjustment of K_1 and K_2 . The transient response is characterized by the settling time T_s and the percent overshoot M_p , while the steady-state behavior is characterized by the oscillation amplitude \tilde{x} of the particle around the node of the standing wave. We define T_s as the time for which the average position of the particle over one period of the acoustic wave remains within $x_f \pm 0.01 \Delta x$, and the percent overshoot M_p as the ratio of the maximum particle overshoot beyond $x = x_f$ and λ .

Figures 2(a)–2(c) show the nondimensional settling time $T_s \omega$, the percent overshoot, and the nondimensional

oscillation amplitude \tilde{x}/λ , each as a function of K_1 , for $\Phi_1 = 0.74$, $\Phi_2 = 0.12$, and $\Phi_3 = -27.56$, which represent a 304 stainless steel, polystyrene, and cork particle in water, respectively. The results are shown for $\Delta x = \lambda/10$. However, T_s , M_p , and \tilde{x} are almost independent of Δx . From Figs. 2(a) and 2(b), we observe that the settling time decreases with increasing K_1 in the overdamped region, while M_p remains zero. The radiation force is small relative to the time-independent Stokes drag force, causing the particle to approach the node slowly, without overshooting it. Increasing K_1 either increases the magnitude of the acoustic radiation force or reduces the time-independent Stokes drag force. This increases the particle velocity as it travels to the node, thus reducing T_s while maintaining $M_p = 0$. Alternatively, in the underdamped region, the magnitude of the acoustic radiation force is large compared to the time-independent Stokes drag force, which causes the particle to overshoot and then oscillate around the node until settling into the steady-state periodic oscillation. Increasing K_1 and, thus, the acoustic radiation force compared to the time-independent Stokes drag force, drives the particle further past the node, increasing M_p while T_s remains constant. While for a second order linear system T_s should remain strictly constant in the underdamped region, Fig. 2(a) indicates a slight decrease in T_s with increasing K_1 . As K_1 increases in the underdamped region, the natural frequency of the fluid-particle system ω_n approaches the operating frequency ω , used to calculate the time averaged particle position. As a result, the time-averaging covers a full period of the harmonic response, filtering out the overshoots and undershoots, and causing the settling time to decrease. From Fig. 2(c), we observe that \tilde{x} increases with K_1 , as expected

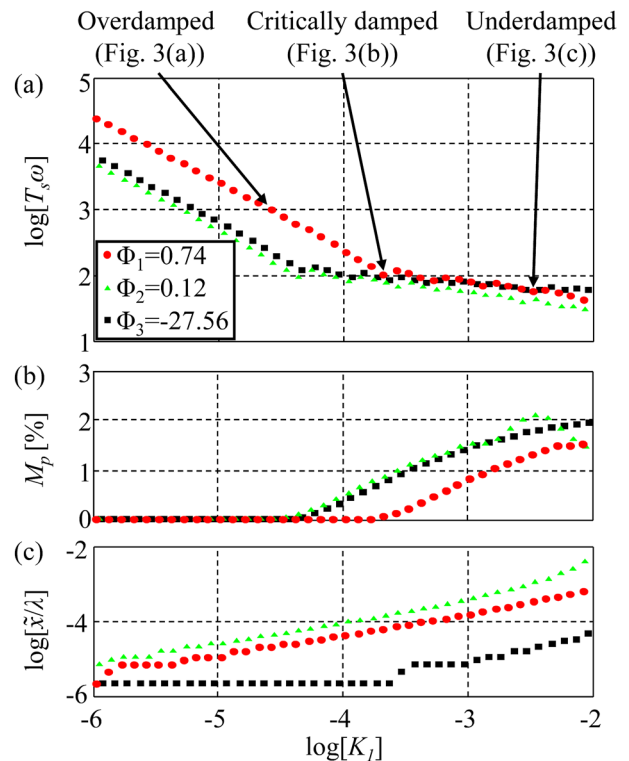


FIG. 2. (a) Nondimensional settling time, (b) percent overshoot, and (c) nondimensional oscillation amplitude, as a function of K_1 , for $\Phi_1 = 0.74$, $\Phi_2 = 0.12$, and $\Phi_3 = -27.56$, and for $\Delta x = \lambda/10$.

for a harmonically forced linear system (Eq. (17)). As K_1 increases, ω_n increases and approaches the operating frequency ω , which results in resonance as the particle absorbs more energy from the oscillating fluid. Hence, increasing K_1 results in a faster particle displacement, at the cost of increasing M_p and \bar{x} .

Figure 3 shows typical particle trajectories $x(t)$ for the (a) overdamped, (b) critically damped, (c) underdamped, and (d) nonlinear cases, for a 304 stainless steel sphere in water ($\Phi_1 = 0.74$), and for $\Delta x = \lambda/10$ and $\omega = 2.1 \times 10^6$ rad/s. The solid-line inset shows a magnified section of the underdamped response, illustrating the harmonic oscillations while the average position of the particle approaches the desired node position. The dashed-line inset shows an enlarged view of the particle trajectory, after it settles into the steady-state oscillation around the node of the standing wave. We observe the steady-state oscillations of the particle due to the oscillating fluid velocity, which applies drag force to the particle surface (see Eq. (11)). In the dashed-line inset, the response is underdamped, and the linear terms in the forcing function dominate, resulting in particle oscillations at the operating frequency ω . Alternatively, the nonlinear response, illustrated in Fig. 3(d) and obtained for high values of K_1 , consists of steady-state oscillations vibrating at multiple frequencies, including ω and its higher harmonics.

Figure 4 shows the nondimensional amplitude of the steady-state particle oscillation as a function of K_2 , which is the ratio of the total time-dependent drag force (Stokes and Oseen) that drives the particle oscillation, and the particle inertia that resists the oscillation. For small values of K_2 the fluid-particle system behaves linearly. Increasing K_2 increases the amplitude of the standing acoustic wave φ_0 , which in turn increases the amplitude of the fluid velocity,

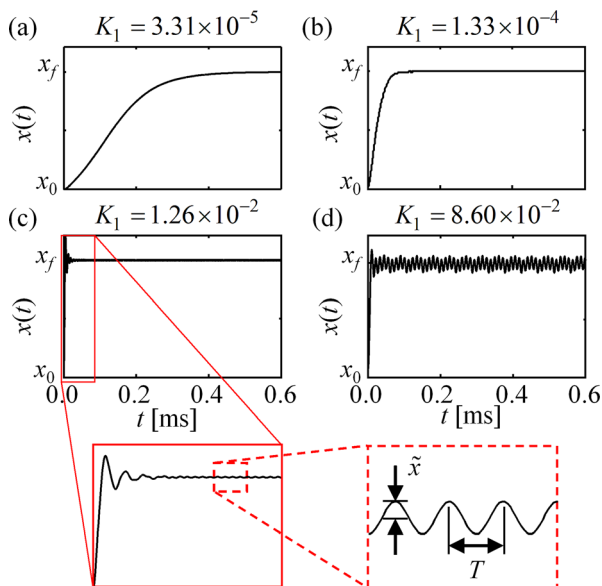


FIG. 3. Typical trajectories of a SS304 sphere submerged in water ($\Phi_1 = 0.74$) as a function of time, for $\Delta x = \lambda/10$ and $\omega = 2.1 \times 10^6$ rad/s, and for different values of K_1 , corresponding to different response regimes: (a) overdamped, (b) critically damped, (c) underdamped, and (d) nonlinear. The solid-line inset shows a magnified view of the harmonic underdamped oscillations as the position settles to the node. The dashed-line inset shows the steady-state oscillations of amplitude \bar{x} around the node, with period T .

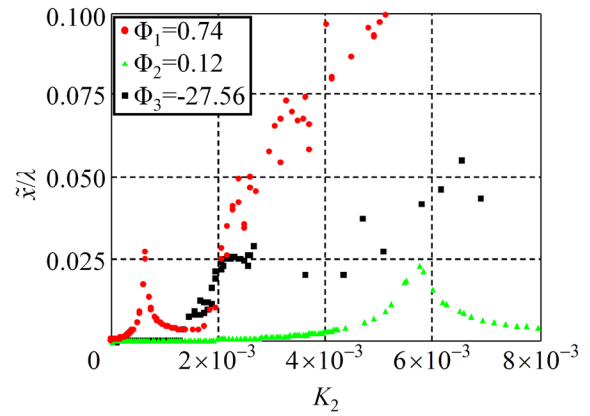


FIG. 4. Nondimensional steady-state oscillation amplitude as a function of K_2 , for $\Phi_1 = 0.74$, $\Phi_2 = 0.12$, and $\Phi_3 = -27.56$.

thereby increasing the drag force acting on the particle and increasing the natural frequency ω_n of the system. As ω_n approaches the operating frequency ω of the standing wave, the system approaches resonance, which increases the steady-state oscillation amplitude. Increasing K_2 further reduces the oscillation amplitude because ω_n diverges from ω . For large values of K_2 , and therefore large velocity differences between the particle and surrounding fluid, the time-dependent Oseen drag force dominates the total time-dependent drag force (Eq. (11)), resulting in nonlinear behavior of the fluid-particle system. Rather than oscillating at a single frequency, the particle oscillates at multiple frequencies (Fig. 3(d)), the amplitude of which increase with increasing K_2 .

In conclusion, we have analyzed the dynamics of a particle submerged in a fluid medium, driven to the node of a standing bulk acoustic wave by an acoustic radiation force. We have simulated the particle trajectory, and have characterized the transient and steady-state behavior of the fluid-particle system as a function of the particle and fluid properties and the operating parameters of the transducers. When the dynamic behavior of the fluid-particle system is overdamped, the settling time decreases and the percent overshoot remains zero, with increasing ratio of acoustic radiation force and time-independent Stokes drag force (K_1). When the dynamic behavior of the fluid-particle system is underdamped, the settling time is constant while the percent overshoot increases with increasing K_1 . We find that the particle oscillates around the node of the acoustic standing wave. Near the node, the amplitude of these oscillations and the natural frequency of the fluid-particle system ω_n are dependent on the ratio of the time-dependent Stokes and Oseen damping forces and the particle inertia (K_2). For small K_2 , the fluid-particle system behaves linearly, oscillating at the operating frequency ω , and resonating as the natural frequency of the system approaches ω . However, for large K_2 the system behaved nonlinearly, oscillating at multiple frequencies, including the operating frequency as well as its higher order harmonics.

J.G. and B.R. acknowledge the support from Army Research Office Contract No. W911NF-14-1-0565.

¹M. Evander and J. Nilsson, *Lab Chip* **12**, 4667 (2012).

²Y. Yamakoshi, Y. Koitabashi, N. Nakajima, and T. Miwa, *Jpn. J. Appl. Phys., Part 1* **45**, 4712 (2006).

- ³Y. Yamakoshi, N. Nakajima, and T. Miwa, *Jpn. J. Appl. Phys., Part 1* **46**, 4847 (2007).
- ⁴B. Raeymaekers, C. Pantea, and D. N. Sinha, *J. Appl. Phys.* **109**, 014317 (2011).
- ⁵J. Greenhall, F. Guevara Vasquez, and B. Raeymaekers, *Appl. Phys. Lett.* **103**, 074103 (2013).
- ⁶X. Chen and R. E. Apfel, *J. Acoust. Soc. Am.* **99**, 713 (1996).
- ⁷T. Kozuka, K. Yasui, A. Towata, and Y. Iida, *Jpn. J. Appl. Phys., Part 1* **46**, 4948 (2007).
- ⁸P. Glynne-Jones, R. J. Boltryk, N. R. Harris, A. W. J. Cranny, and M. Hill, *Ultrasonics* **50**, 68 (2010).
- ⁹C. R. P. Courtney, C. K. Ong, B. W. Drinkwater, A. L. Bernassau, P. D. Wilcox, and D. R. S. Cumming, *Proc. R. Soc. London, Ser. A* **468**, 337 (2012).
- ¹⁰A. Grinenko, C. K. Ong, C. R. P. Courtney, P. D. Wilcox, and B. W. Drinkwater, *Appl. Phys. Lett.* **101**, 233501 (2012).
- ¹¹J. J. Faran, *J. Acoust. Soc. Am.* **23**, 405 (1951).
- ¹²O. A. Sapozhnikov, *J. Acoust. Soc. Am.* **133**, 661 (2013).
- ¹³P. J. Westervelt, *J. Acoust. Soc. Am.* **23**, 312 (1951).